A Simulation-Based Framework for Structural Loads Assessment during Dynamic Maneuvers

Gael Goron* , Ruxandra Duca* , Darshan Sarojini* , Somil R. Shah*

Imon Chakraborty† , Simon Briceno‡ , Dimitri N. Mavris§

Aerospace Systems Design Laboratory, School of Aerospace Engineering

Georgia Institute of Technology, Atlanta, Georgia, 30332

Federal Aviation Regulations pertaining to structural integrity are key drivers in aircraft design and certification, and often involve critical loads occurring during dynamic maneuvers. In the context of increasing costs of testing and the general trend towards parametric design, there is a need for a more thorough consideration of such dynamic load cases earlier in the design process. In this work, a simulation framework is introduced to assess structural requirements stemming from such dynamic load conditions. Relevant aspects of the dynamics of the aircraft, the control system, and the pilot are modeled in order to simulate the maneuver and thereafter obtain inertial and aerodynamic loads on the empennage during the simulated maneuver. The loads are then translated into structural shear forces and bending moments through structural post-processing routines. This approach is demonstrated for the case of a representative business jet during the checked pitch maneuver. The analyses are repeated for three weight conditions and over the flight envelope for the aircraft from which the load cases resulting in the most constraining loads are determined.

I. Introduction and Background

Certification requirements are key drivers during the aircraft design process. Through computational analyses, flight tests, and extensive ground testing, the manufacturer gains confidence that the aircraft structure is able to sustain potential loads as prescribed in regulatory standards. This is required for the design to be deemed safe, durable, and reliable.[1,2]

In the United States, regulations dealing with loads that the aircraft must be designed for come from the Federal Aviation Administration (FAA) in the form of Federal Aviation Regulations (FARs). FARs pertaining to structural loads and integrity are among the most stringent. New requirements are continually updated to deal with new accidents or new aircraft features. One example of this is the recent update to gust and turbulence loads regulations, where large amounts of airline data have been used to modify the gust intensities.[3] Described in Title 14 of the Code of Federal Regulations, Part 25 (14 CFR §25), the airworthiness standards for transport category airplanes include structural design requirements that are usually analyzed and validated using a building block approach.[4] Results are gathered analytically at the element level, then turned into evidence through testing at the sub-component and component levels.[1] Although full-scale testing is required,[5] much of the intermediate or sub-component testing could be reduced by using computational analyses, thus reducing time and costs.

A key enabler for such a simulation-assisted certification approach is the ability to simulate complex, dynamic maneuvers to determine the resulting critical structural loads on the airframe. Calculating critical loads is a multidisciplinary process which entails simulating the aircraft dynamics corresponding to the prescribed FAR maneuver for different flight conditions within the flight envelope and identifying the most

*Graduate Research Assistant, ASDL, School of Aerospace Engineering, Georgia Tech, AIAA Student Member

†Research Engineer II, ASDL, School of Aerospace Engineering, Georgia Tech, AIAA Member

‡Research Engineer II, ASDL, School of Aerospace Engineering, Georgia Tech, AIAA Senior Member

§S.P. Langley Distinguished Regents Professor and Director of ASDL, Georgia Tech, AIAA Fellow

severe loads. To this end, a maneuver simulation capability is developed, comprising of modules for aerodynamics, propulsion, mass properties, the flight control system, and pilot action, with the goal of simulating the aircraft's motion history during dynamic maneuvers. In parallel, a structural loads assessment capability is developed which uses the motion history to determine both the gross and distributed aerodynamic and inertial loads experienced by the structure during the course of the maneuver.

To demonstrate this framework, the checked pitch maneuver, described in FAR §25.331(c)(2)[6] is chosen. The goals of the simulation capability are to simulate the maneuver in accordance with the FAR to calculate the critical horizontal tail root loads (bending moment, torsional moment, and shear forces) as well the corresponding elevator hinge moment. The proposed approach was developed and tested using data corresponding to an aircraft from the Gulfstream Aerospace Corporation's product line. The results presented in this paper have been suitably modified where necessary in order to protect proprietary data corresponding to this aircraft's aerodynamics, mass properties, geometry, and performance envelope.

The remainder of this paper is organized as follows: Section II presents the simulation model integrating the FAR and the flight dynamics. Section III describes the structural loads analyses which process the time histories obtained in the simulation model. Section IV presents and describes the results of the work for several test cases. Finally, Section V provides a summary of the work and suggests multiple avenues of future work.

II. FAR-Based Flight Simulation Model

The objective of the flight simulation model is to simulate the aircraft dynamics corresponding to maneuvers and flight conditions specified in the FARs. It is comprised of the following three main elements, which are described in greater detail in the following sections:

A. Aircraft Model: This contains modules for aerodynamics, propulsion, mass properties, and the flight control system.

B. Pilot Model: This emulates the actions of a human pilot attempting to track a commanded state or control trajectory, subject to permissible effort constraints.

C. FAR-Based Maneuver Control Logic: Depending on the evolution of the maneuver and the particular FAR being analyzed, this element generates the relevant state or control trajectories to be tracked by the pilot model.

II.A. Aircraft Model

The simulation is developed using MATLAB/Simulink, and makes extensive use of the *Aerospace Blockset*. It customizes and extends a previously developed simulation capability[7] to meet the requirements of the current problem. A high-level view of the Simulink model is shown in Figure 1. Within the aircraft model, the model of the flight control system uses the pilot inputs as well as the hinge moments developed at the control surfaces to determine the actual control surface motion. The aircraft model is also responsible for the evaluation of forces and moments acting on the aircraft, which are then used to integrate the equations of motion to simulate its dynamics.

The forces and moments acting on the vehicle are the net result of aerodynamic ($\vec{F}_{aero}$, $\vec{M}_{aero}$), propulsive ($\vec{F}_{prop}$, $\vec{M}_{prop}$), and gravitational ($\vec{F}_{grav}$, $\vec{M}_{grav}$) forces and moments:

$$\vec{F}_{total} = \vec{F}_{aero} + \vec{F}_{prop} + \vec{F}_{grav} \tag{1}$$

$$\vec{M}_{total} = \vec{M}_{aero} + \vec{M}_{prop} + \vec{M}_{grav} \tag{2}$$

Since the checked pitch maneuver is purely longitudinal, only the blocks responsible for modeling the longitudinal dynamics are relevant to the problem. All moments are taken about a fixed reference point O: $\vec{r}_O = \{x_{ref}, y_{ref}, z_{ref}\}^T$. Following established convention, forces and moments are expressed in the body-fixed frame whose x-axis points towards the nose of the aircraft, y-axis points towards the starboard wing, and z-axis points downward. Also following convention, the subsequent structural loads analyses use a body-fixed frame where the x-axis points aft and the z-axis points upward. A 180° rotation about the y-axis is used to transfer relevant vector quantities between these two axis systems. The subsequent sections describe the modeling approach and assumptions pertaining to the following aspects of the aircraft model:

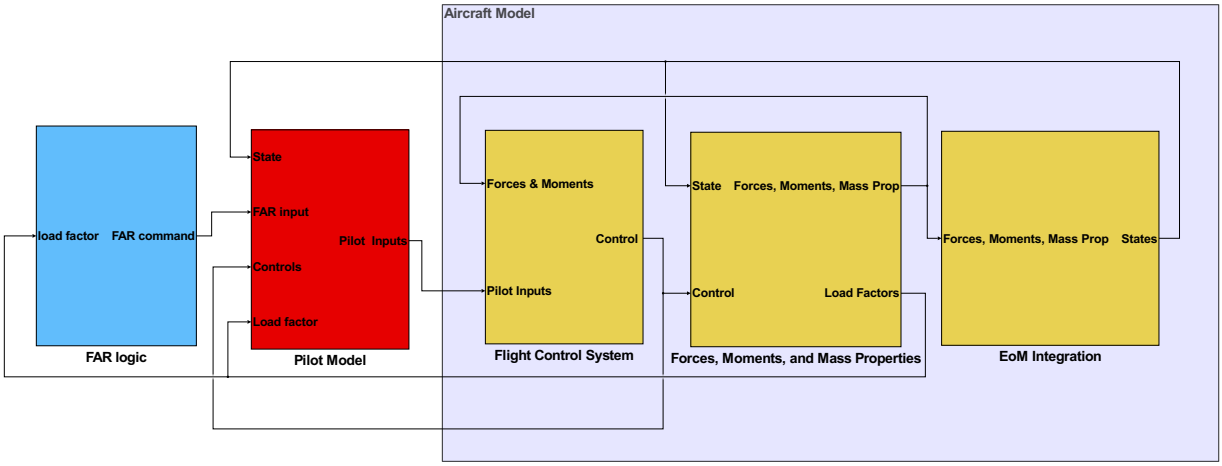

Figure 1: Simulink flight simulation framework

1. Aerodynamics
2. Propulsion
3. Mass Properties
4. Equations of Motion
5. Flight Control System
6. Trim Solution

II.A.1. Aerodynamics

The aerodynamic force can be expressed in the body-fixed axes in terms of the normal force N, axial force A, and the side force Y.

$$\vec{F}_{aero} = \begin{bmatrix} A \\ Y \\ N \end{bmatrix} \tag{3}$$

Since the lateral dynamics are not relevant to this problem, the side force $Y \equiv 0$. The net aerodynamic normal force N is modeled as the sum of the tail-off contribution N_{wb} and the isolated tail contribution N_t.

$$N = N_{wb} + N_t, \tag{4}$$
$$N_{wb} = \bar{q}S(C_{N_0} + C_{N_\alpha}\alpha), \tag{5}$$
$$N_t = \bar{q}S(C_{N_{\alpha_{tail}}}\alpha_{tail} + C_{N_{\delta_e}}\delta_e), \tag{6}$$

where $\bar{q}$ is the dynamic pressure, α is the aircraft angle of attack, α_{tail} is the incidence angle seen by the horizontal stabilizer, and δ_e is the elevator deflection. The planform area of the wing S is used as the reference area for the aerodynamic coefficients $C_{N_{(.)}}$.

The downwash is modeled as a first order linear model in angle of attack, $\epsilon = \epsilon_0(M) + \epsilon_\alpha(M)\,\alpha$ with both $\epsilon_0(M)$ and $\epsilon_\alpha(M)$ being functions of the Mach number M. The angle of attack at the tail, α_{tail} is obtained by accounting for the aircraft angle of attack α, stabilizer setting angle i_t, downwash ϵ, and the incremental incidence angle $(q\ell_t/V)$ generated due to pitch rate q:[8]

$$\alpha_{tail} = \alpha + i_t - \epsilon + \frac{q\ell_t}{V} \tag{7}$$
$$= \alpha + i_t - \epsilon_0 - \epsilon_\alpha\alpha + \frac{q\ell_t}{V} \tag{8}$$
$$= \alpha(1 - \epsilon_\alpha) + i_t - \epsilon_0 + \frac{q\ell_t}{V} \tag{9}$$

The build-up of the aerodynamic pitching moment about the reference point follows similarly and is given by

$$M_{aero} = M_{wb} + M_t, \tag{10}$$
$$M_{wb} = \bar{q}Sc(C_{m_0} + C_{m_\alpha}\alpha), \tag{11}$$
$$M_t = \bar{q}Sc(C_{m_{\alpha_{tail}}}\alpha_{tail} + C_{m_{\delta_e}}\delta_e), \tag{12}$$

where the coefficients $C_{m_{(.)}}$ are non-dimensionalized using reference area S and mean aerodynamic chord c.

The most significant contributor to the aerodynamic axial force A is the aerodynamic drag experienced by the aircraft. However, no drag data was used in the aerodynamic modeling, due to its highly sensitive nature. Instead, the NASA legacy software, *Flight Optimization System (FLOPS)*, is used to compute drag polars at different Mach and altitude configurations, but using only the basic geometry and configuration of the aircraft. These drag characteristics are then projected along the body-fixed axes for use in the simulation. The drag estimation process is represented in Figure 2, in which the lift coefficient C_L is obtained from the z wind axis force equation, using the current state of the aircraft and other forces.

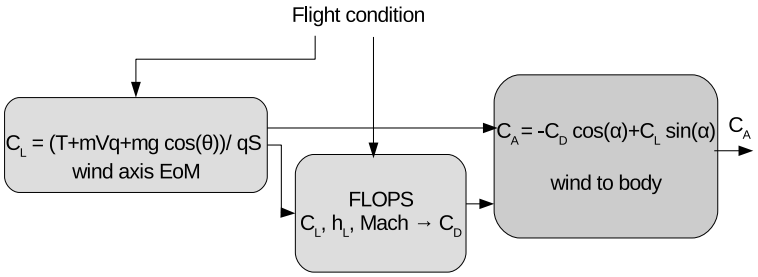

Figure 2: Process to estimate axial aerodynamic force

II.A.2. Propulsion

The thrust force, assumed parallel to the body-fixed x-axis, is modeled using a linear relationship between the minimum thrust T_{min} (idle power setting) and the maximum thrust T_{max} (full power setting). The minimum and maximum thrust, which are functions of altitude and Mach number, are queried from look-up tables. The net thrust force is then obtained as

$$T(\tau, h, M) = T_{min}(h, M) + \tau\left\{T_{max}(h, M) - T_{min}(h, M)\right\}, \tag{13}$$
$$\vec{F}_{prop} = \begin{bmatrix} T(\tau, h, M) \\ 0 \\ 0 \end{bmatrix}, \tag{14}$$

where τ is the throttle setting , h is the altitude above mean sea level, and M is the Mach number. The moment due to thrust about the reference point is then simply obtained by taking the cross product, as shown.

$$\vec{M}_{prop} = \vec{r}_T \times \vec{F}_{prop} \tag{15}$$

where the moment arm $\vec{r}_T$ is a vector from the reference point O to the thrust application point.

II.A.3. Mass Properties

Noting that the checked pitch maneuver is conducted with wings level (bank angle $\phi \equiv 0$), the gravitational force is resolved along the body-fixed axes using only the pitch angle θ, while the corresponding moment is computed about the reference point O using the moment arm $\vec{r}_g$ running from O to the center of gravity (CG) of the aircraft. Thus,

$$\vec{F}_{grav} = \begin{bmatrix} -Mg\sin(\theta) \\ 0 \\ Mg\cos(\theta) \end{bmatrix}, \tag{16}$$

$$\vec{M}_{grav} = \vec{r}_g \times \vec{F}_{grav}, \tag{17}$$

where g is the acceleration due to gravity.

Given the duration of the checked pitch maneuver (order of seconds), no variation of aircraft mass due to fuel consumption is modeled, and a constant mass is assumed. The same argument applies to the aircraft inertia tensor, whose elements are computed with respect to the reference point and expressed in the body-fixed axis system.

$$\bar{\bar{I}} = \begin{bmatrix} I_{xx} & I_{xy} & I_{xz} \\ I_{yx} & I_{yy} & I_{yz} \\ I_{zx} & I_{zy} & I_{zz} \end{bmatrix} \tag{18}$$

While the mass and inertia tensor do not vary over the course of a particular simulation, simulations are performed for three distinct loadouts (described subsequently) which vary with regard to mass, CG location, and components of the inertia tensor.

II.A.4. Equations of Motion

The equations of motion block is similar to the existing *Custom Variable Mass 6DOF (Euler Angles)* block within the *Aerospace Blockset*, but the equations are cast about a fixed reference point O rather than the CG. This enables, for instance, the dynamics of a moving CG (e.g., due to decreasing fuel mass or fuel transfer) to be modeled. The force and moment equations in vector form are given below.

$$\vec{F}_{total} = m\left(\dot{\vec{V}}_0 + \vec{\omega} \times \vec{V}_0 + \ddot{\vec{r}}_g + \dot{\vec{\omega}} \times \vec{r}_g + 2\,\vec{\omega} \times \dot{\vec{r}}_g + \vec{\omega} \times (\vec{\omega} \times \vec{r}_g)\right), \tag{19}$$

$$\vec{M}_{total} = \bar{\bar{I}}\dot{\vec{\omega}} + \vec{\omega} \times \bar{\bar{I}}\omega + m\,\vec{r}_g \times \left(\dot{\vec{V}}_0 + \vec{\omega} \times \vec{V}_0\right), \tag{20}$$

where, in addition to previously defined quantities, $\vec{V}_0 = \{u, v, w\}^T$ is the velocity of the reference point O and $\vec{\omega} = \{p, q, r\}^T$ is the angular velocity of the aircraft. The more specific case where the reference point O coincides with the CG can be obtained by setting $\vec{r}_g = 0$ in the above. Kinematic relationships are used to obtain the derivatives of the Euler angles ϕ, θ, and ψ from the angular rates p, q, and r, and also derivatives of the position x_0, y_0, and z_0 of the reference point O from the velocities u, v, and w. The resulting system of 12 nonlinear ordinary differential equations (in $u, v, w, p, q, r, \phi, \theta, \psi, x_0, y_0, z_0$) for six degrees-of-freedom rigid body motion is numerically integrated to obtain the motion history of the aircraft during the maneuver.

II.A.5. Flight Control System Dynamics

The checked pitch maneuver requirements are specified in terms of yoke deflection, with restrictions on the maximum permissible pilot force needed to achieve said deflections. To link the pilot force on the control column to the elevator deflection and to capture feedback loads from the elevator back to the yoke, a simplified model for the elevator control system is implemented. The model features a mechanical linkage accompanied by a hydraulic booster. The goal of this model, which is shown in Figure 3, is to obtain a relationship between the pilot force and the elevator deflection. The linear position x_{yoke}, velocity $\dot{x}_{yoke}$, and acceleration $\ddot{x}_{yoke}$ of the yoke are mapped to corresponding angular quantities δ_e, $\dot{\delta}_e$, and $\ddot{\delta}_e$ for the elevator by assuming a simplified constant gearing ratio G, such that

$$G = \frac{\ddot{\delta}_e}{\ddot{x}_{yoke}} = \frac{\dot{\delta}_e}{\dot{x}_{yoke}} = \frac{\delta_e}{x_{yoke}} \tag{21}$$

The translational motion of the yoke is governed by

$$m\ddot{x}_{yoke} = F_{pilot} - F_{system} - c_\ell\,\dot{x}_{yoke}, \tag{22}$$

where m is the effective translating mass of the control system, c_ℓ is used to model translational friction losses, F_{pilot} is the force applied by the pilot on the yoke, and F_{system} is the effective force transmitted into the input linkage of the control system. The hydraulic booster is assumed to generate a proportional force $F_{booster} = kF_{system}$ which adds to the input force, yielding a net actuating force $F_c = (1 + k)F_{system}$. For

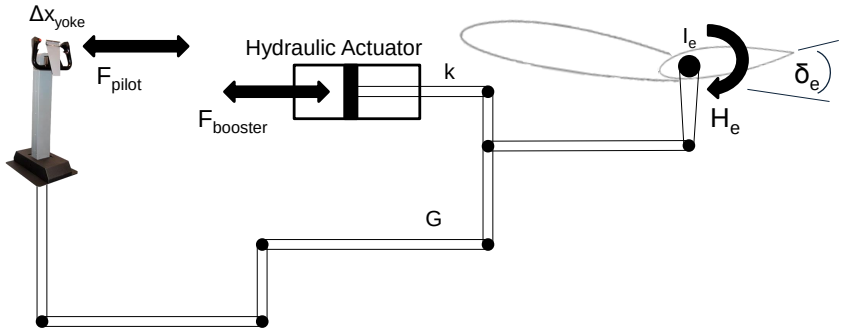

Figure 3: Simplified model of hydraulically-boosted elevator control system

simplicity, the dynamics of the booster are neglected. Taking into account the gearing ratio G, the actuating moment generated about the elevator hinge line by the net force is given by

$$M_c = (1+k)\frac{F_{system}}{G}. \tag{23}$$

The motion of the elevator is governed by

$$I_e\ddot{\delta}_e = M_C + H_e - c_r\dot{\delta}_e, \tag{24}$$

where I_e is the moment of inertia of the elevator about the hinge line, c_r is used to model rotational friction losses, and H_e is the aerodynamic hinge moment. Combining Eqs. 21 - 24 yields the following second-order ordinary differential equation for the motion of the elevator:

$$\left[I_e + \frac{m(1+k)}{G^2}\right]\ddot{\delta}_e + \left[c_r + \frac{c_\ell(1+k)}{G^2}\right]\dot{\delta}_e = F_{pilot}\left[\frac{1+k}{G}\right] + H_e \tag{25}$$

The aerodynamic hinge moment H_e appearing in Eq. 25 is modeled as a function of tail incidence angle α_t, elevator deflection δ_e, and trim tab deflection δ_{tab} as

$$H_e = H_{e_{\alpha_t}}\alpha_t + H_{e_{\delta_e}}\delta_e + H_{e_{\delta_{tab}}}\delta_{tab}, \tag{26}$$

in which the hinge moment coefficients $H_{e_{(.)}}$ are obtained from lookup tables.

II.A.6. Trim Solution

To initialize the maneuver simulation, the aircraft is assumed to be flying at steady level flight, as per FAR requirements. The aircraft is trimmed only with the elevator control. To solve for the trim parameters: angle of attack (α), elevator deflection (δ_e), and throttle setting (τ), the total force on the body x and z axes as well as the pitching moment must be zero. This yields the following system of trim equations.

$$T(\tau, h, M) - A - mg\sin(\alpha) = 0, \tag{27}$$

$$N(\alpha, \delta_e) - mg\cos(\alpha) = 0, \tag{28}$$

$$M_{prop}(\tau) + M_{grav} + M_{aero}(\alpha, \delta_e) = 0, \tag{29}$$

where all dependencies to the trim variables are shown and the moments in Eq. 29 are the y body axis components of the vectors given in Eqs. 10, 15, and 17. It should also be noted that for steady, level, trimmed flight with $\gamma = 0$, $\theta = \alpha$.

This set of equations is of the form $\mathcal{X}(\tau, \alpha, \delta_e) = 0$ and is therefore a root finding problem. The system is solved using the trust region Dogleg root finding method implemented in the MATLAB routine *fsolve*. Additionally, on this aircraft, an elevator trim tab allows to cancel out the hinge moment in the trim configuration. Therefore, once the angle of attack, elevator deflection, and throttle setting values at trim are obtained, the elevator tab deflection δ_{tab} can be solved for with Equation 26.

$$\delta_{tab,trim} = -\frac{H_{e_{\delta_e}}\delta_{e,trim} + H_{e_{\alpha_t}}\alpha_{tail,trim}}{H_{e,tab}} \tag{30}$$

For starting airspeeds in excess of the aircraft's maximum level-flight airspeed, the trim solution is still obtained by allowing the throttle position to be greater than 1.0. Once the system of equations above is solved for all test points in the flight envelope, the trim solution is used to initialize the simulation. Figure 4 shows the variation of the four trimmed quantities over the flight envelope.

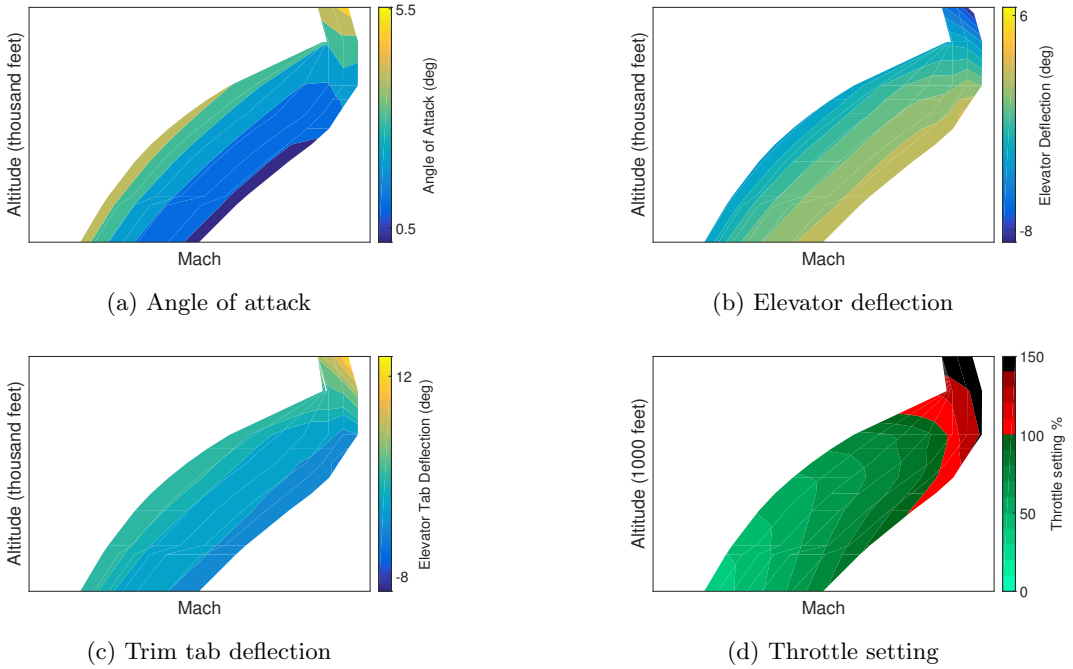

(a) Angle of attack

(b) Elevator deflection

(c) Trim tab deflection

(d) Throttle setting

Figure 4: Trim angle of attack, elevator deflection, trim tab deflection, and throttle setting for heavyweight configuration

II.B. Pilot Model

The tracking actions of the human pilot are modeled using a proportional-integral-derivative (PID) controller that attempts to match the actual flight deck pitch control deflection with the deflection specified in FAR §25.331(c)(2) for the maneuver. Therefore, the error e for the PID controller is given as the difference between the commanded pitch control deflection $\delta_{e,cmd}$ from the FAR and the actual pitch control deflection δ_e:

$$e = \delta_{e,cmd} - \delta_e \tag{31}$$

Using this error signal definition, the PID controller is implemented in the Simulink model with proportional (K_P), integral (K_I), and derivative (K_D) gains to obtain the pilot's applied force F as

$$F(e) = K_P e + K_I \frac{1}{s} e + K_D \frac{N}{1 + N\frac{1}{s}} e, \tag{32}$$

where the filter coefficient N is set to a default value of 100. The dynamics of the flight control system vary with the flight condition, especially due to the variation of the elevator hinge moment magnitudes with dynamic pressure. Therefore, all the PID gains are first tuned manually for extreme conditions of high and low Mach number and altitude. Then, the gains are scheduled as a function of dynamic pressure using a lookup table.

The output of the pilot model is the pilot force F required to minimize the error between the commanded pitch control deflection $\delta_{e,cmd}$ and the actual deflection δ_e. One of the main benefits of modeling the pilot force is the ability to capture maximum pilot effort as described in FAR §25.397. These limits are modeled by saturating the output of the PID block, limiting the maximum magnitude of force that can be applied by the pilot to 300 lbf in the simulation.

II.C. Checked Pitch Maneuver Logic and Implementation

The checked pitch maneuver (nose up or nose down) consists of a pitching motion of the aircraft generated through control input from the pilot which is then checked, or stopped with opposite control input. The maneuver is precisely described in the text of FAR §25.331(c)(2) in terms of control deflection as a function of time, achieved load factor, and pilot force. The function that describes the yoke displacement over time is given as[6]

$$\delta(t) = \delta_{max} \sin(\omega t), \quad \text{for} \quad 0 \leq t \leq t_{max} \quad \text{and} \quad \omega \leq \omega_{max} \tag{33}$$

with:

- δ_{max}: the maximum yoke deflection, as limited by the control system stops, control surface stops, or by pilot effort as prescribed in FAR §25.397.
- $t_{max} = \frac{3\pi}{2\omega}$
- ω: circular frequency (rad/sec) of the control deflection taken equal to the undamped natural frequency of the short period rigid mode of the airplane, with active control system effects included where appropriate.
- $\omega_{max} = \frac{\pi V}{2V_A}$: with V the speed of the airplane at entry of the maneuver and V_A the design maneuvering speed.

Equation 33 is modified to account for achievable load factors. If the maximum load factor is not reached with the control input specified by Eq. 33, then the pilot must hold the control surface deflected until the load factor is reached but for no more than five seconds. On the other hand, the maximum prescribed positive load factor must not be exceeded. In such cases, the flight deck pitch control deflection amplitude should be scaled down. Figure 5 shows examples of these types of longitudinal control inputs.

Furthermore, the loads do not need to be recorded after the time for which the load factor goes below zero (respectively above 2.5) during the second phase of the nose up (respectively nose down) maneuver, in which case the simulation can be stopped. Also, the simulation may be stopped if the effort required by the pilot to control the airplane falls outside the ranges prescribed by FAR §25.397. For this work, the upper bound of 300 lbf is employed.

Simulations must be performed for maneuver entry speeds between the design maneuvering speed V_A and the design dive speed V_D. In order to correctly implement FAR §25.331(c)(2), the checked pitch maneuver must then be performed for several points in the aircraft flight envelope corresponding to speeds between those two values. The flight condition is defined by the entry speed, starting altitude, and loadout of the aircraft (weight and CG position). For each flight condition, the dynamics of the aircraft are different. Consequently, both the circular frequency of the control input ω and the maximum control deflection δ_{max} need to be computed for each case in order to generate the appropriate control input for the pilot.

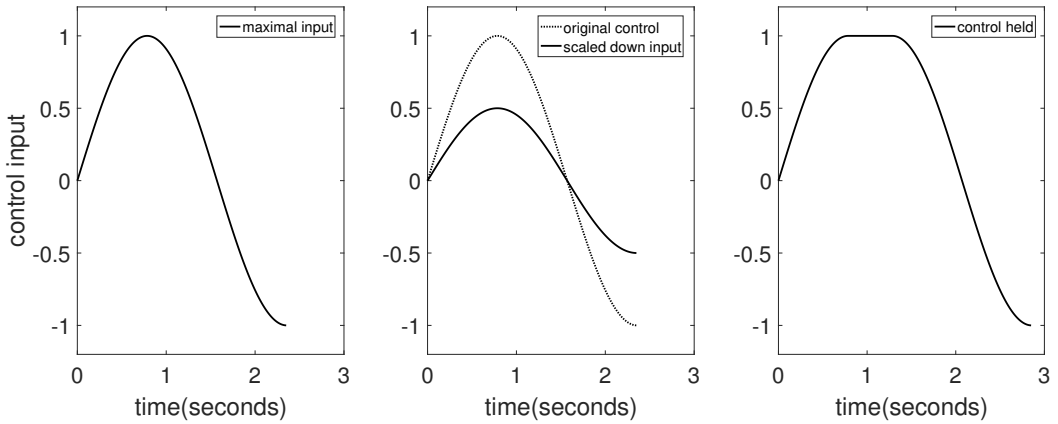

Figure 5: Examples of control inputs. Left: Prescribed sinusoidal control input; Center: Control input scaled down to avoid exceeding limit load factor; Right: Full control input held to allow load factor to build

II.C.1. Testing Envelope

Since FAR §25.331(c)(2) specifies that the checked pitch maneuver is to be performed at speeds between the maneuvering speed V_A and the dive speed V_D, the Mach-altitude flight envelope was discretized to obtain a sufficient representation of all altitude and speed combinations. This process was started with known values for cruise speed and dive speed at all altitudes. The true maneuver airspeed V_A was calculated at each of these altitudes as

$$V_A = \sqrt{\frac{2Wn^+}{C_{N_{max}}\rho S}}. \tag{34}$$

Here, $C_{N_{max}}$ has a dependency on Mach number (therefore, speed), and thus an iterative solution is required to compute maneuver true airspeed V_A. The density ρ depends on the altitude, while the weight W depends on the weight condition being considered. S is the reference wing planform area while n^+ is the positive limit load factor. Performing this calculation for all altitudes of interest yields the left limit of the testing envelope. The right boundary consists of the design dive speed V_D. Then, for each altitude, 7 points were considered, including V_A, V_C, and V_D as seen in the Figure 6. In general, the dynamic response of the aircraft will vary with loadout (weight and CG position). In this work, simulations are performed for three weight conditions which are described in Table 1. Condition 1 is a representative nominal loadout while Conditions 2 and 3 represent respectively a heavy loadout with a forward CG and a light loadout with an aft CG. The altitudes, Mach numbers, and weight configurations taken together resulted in a total of 231 test cases.

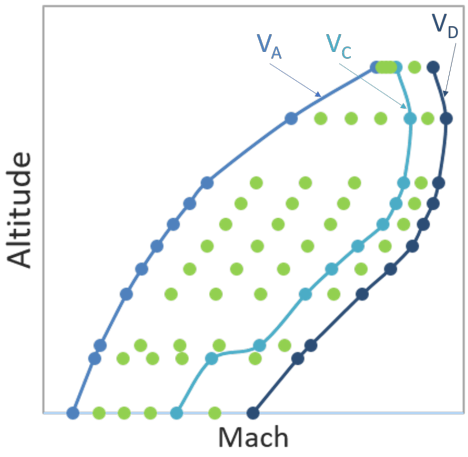

Figure 6: Maneuver testing envelope discretized into analysis points

Table 1: Weight configurations

Condition	**Weight**	**CG Location**
1	Mission	Design
2	Heavyweight	Forward
3	Lightweight	Aft

II.C.2. Simulation Process Overview

Figure 7 shows a flowchart that summarizes the overall process for the FAR-driven flight simulation for a single case from the testing envelope. It is created using an Extended Design Structure Matrix (xDSM).[9] Each analysis is on the diagonal, inputs to the analysis are on the corresponding column, and outputs from the analysis are on the corresponding row. Starting with an altitude, Mach number and weight configuration, the trim algorithm is run to determine the trim controls to put the airplane in steady, level flight. At this point, an impulse control input (described in Section II.C.3) allows for the determination of the short period characteristics. Once the circular frequency of the FAR control input has been set, an iterative process

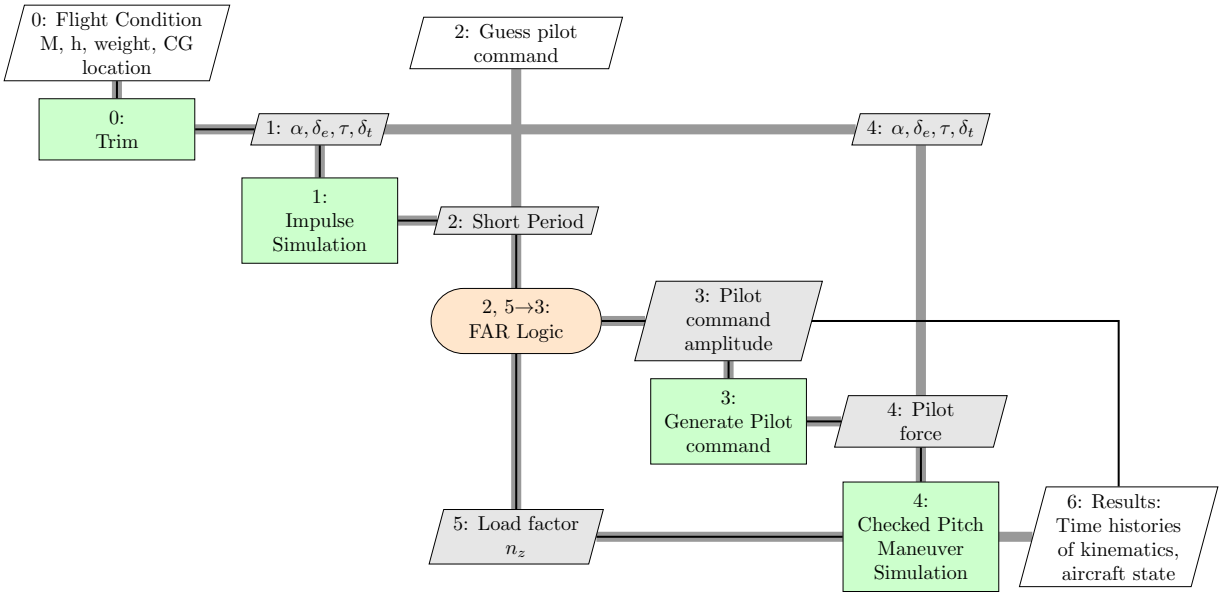

Figure 7: Maneuver simulation flowchart

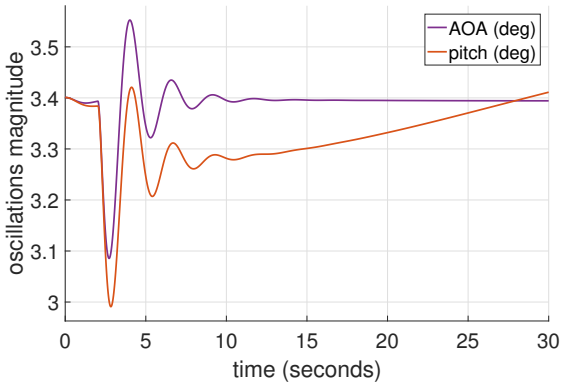

Figure 8: Angle of attack and pitch angle response to an elevator impulse

(described in Section II.C.4) is necessary to comply with the FAR requirements on the maximum (for nose up maneuver) or minimum (for nose down maneuver) achieved load factor. This is represented by the $2, 5 \rightarrow 3$ loop in the flowchart. The goal of this iterative process is to determine the flight deck pitch control input for the pilot which complies with FAR §25.331(c)(2) as described in Eq. 33 and Figure 5. Finally, once the correct pitch control input has been established, a final checked pitch maneuver is run, and all the quantities of interest are recorded during the course of the maneuver.

II.C.3. Short Period Evaluation

Since the short period characteristics vary with CG position and dynamic pressure,[10] for each analysis point in Figure 6, the short period undamped natural frequency ω_n and damping ratio ζ are estimated. The short period mode is excited with an impulse or a short step (less than a second) in the elevator control input.[11] Therefore, for each point, the pitch response of the airplane is recorded after an impulse in elevator command in order to evaluate both ω_n and ζ. Figure 8 shows an example of pitch angle and angle of attack responses following an elevator impulse. The response is analyzed as a generic second order dynamic system response,

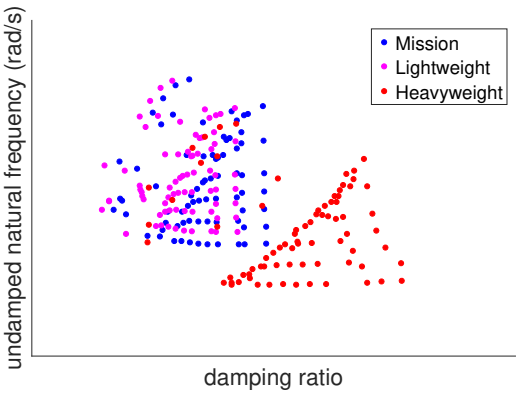

Figure 9: Short period characteristics for all cases in the flight envelope

where, if x_1 and x_2 are the amplitudes of the first and second peak, then w_n and ζ are given by

$$\zeta = \frac{\Delta/2\pi}{\sqrt{1+(\Delta/2\pi)^2}},$$
$$\omega_n = \omega_d\sqrt{1+(\frac{\Delta}{2\pi})^2}, \tag{35}$$

where, ω_d is the circular frequency observed in the response and Δ is the quantity $\ln(\frac{x_1}{x_2})$. The undamped natural frequency and damping ratio for all test points are shown in Figure 9.

II.C.4. Amplitude Scaling Routine

Once the circular frequency ($\omega = \omega_n$) for the short period mode is known, the checked pitch maneuver can be simulated. However, for certain cases in the flight envelope, the amplitude of the deflection must be scaled down so as to not exceed 2.5 g for the nose up maneuver or fall below 0 g for the nose down maneuver. For all cases, the checked pitch maneuver simulation is run with several amplitude factors k_{amp} such that $\delta(t) = \delta_{av}k_{amp}\sin(\omega t)$, where $\delta_{av} = |\delta_{max} - \delta_{e,trim}|$ is the available elevator authority accounting for elevator travel limits and the elevator angle at trim. The peak load factor is then recorded as a function of the amplitude factor.

After an initial run with a very small amplitude, $k_{amp} = 0.1$, the amplitude factor is then corrected by a simple scale $\frac{2.5}{n_{peak}}$ for the nose up maneuver and $\frac{1}{|n_{peak}|}$ for the nose down maneuver. The test points considered required either one or two scaling iterations in order to settle on the desired maximum load factor, yielding the amplitude scaling factor solutions shown in Figure 10.

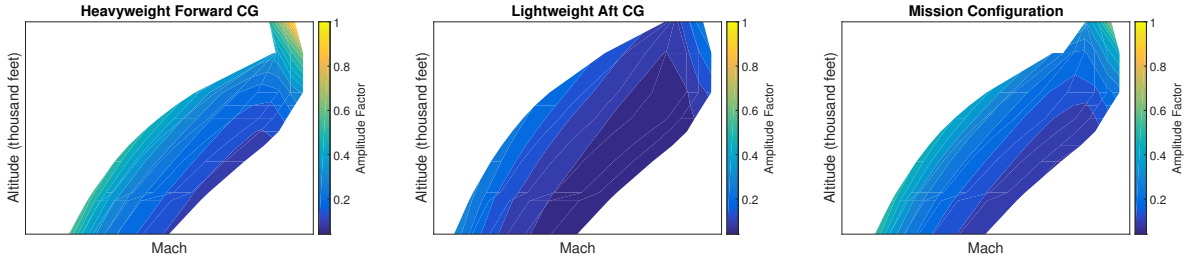

Figure 10: Amplitude scaling factor for the three weight conditions

III. Structural Loads Analysis

The goal of the structural loads analysis is to compute the structural loads (axial force, shear forces, and bending moments) on the horizontal tail due to the inertial and aerodynamic forces and moments generated

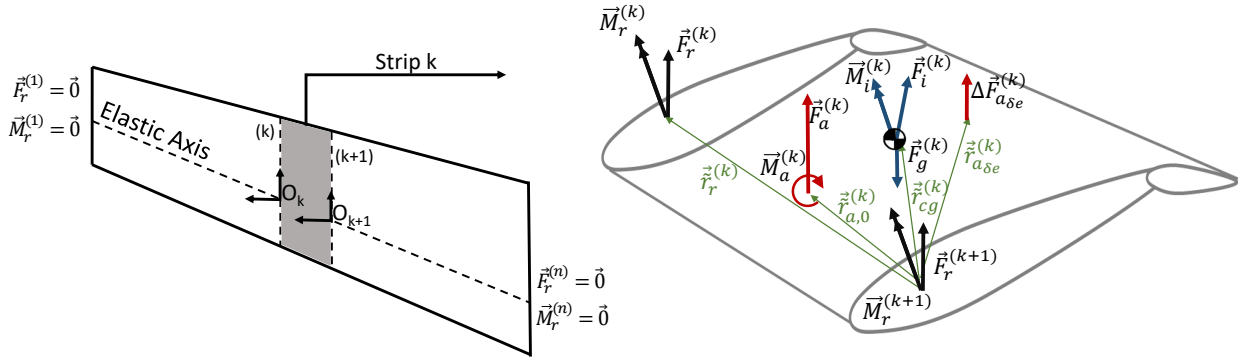

Figure 11: Strip method - applying dynamic equilibrium on each strip to obtain reaction loads

during the maneuver. In particular, the loads at the tail root on the elastic axis are of interest. The proposed method involves dividing the horizontal tail into sections or "strips", with known aerodynamic characteristics and mass properties, and calculating the forces and moments that develop on each strip at each time step. Hence, this computation relies primarily on the time histories of aircraft states obtained from the maneuver simulation, including aircraft attitude, control surface and tab position, and atmospheric data. Dynamic equilibrium criteria are applied on each strip, starting from the tip and moving towards the root, and computing the action/reaction loads at the strip boundaries. This approach takes advantage of the fact that the reaction loads at the outboard tip of the stabilizer are zero, allowing for the calculation of loads on the inboard boundary of the outboard-most strip. This procedure, represented in Figure 11, is then continued while moving successively inward until root loads for the horizontal tail can be eventually computed. A high-level flowchart (Figure 12) is created using an Extended Design Structure Matrix (xDSM) to show dataflow. The following sections give an in-depth explanation of how these computations are carried out.

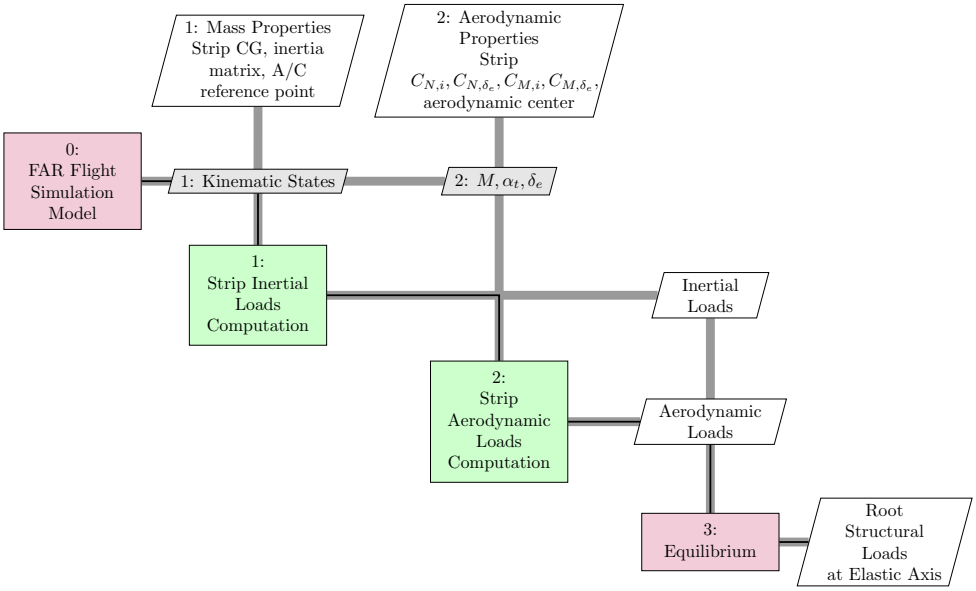

Figure 12: Structural loads analysis flowchart

III.A. Strip-Wise Equilibrium

The strip method entails knowing reaction forces and moments at one strip boundary, as well as forces and moments acting on the strip itself, then computing reactions at the other boundary by imposing dynamic

equilibrium. Figure 11 shows a strip 'k' with the aerodynamic force $\vec{F}_{a,0}^{(k)}$ (with faired elevator), the incremental change in aerodynamic force due to elevator deflection $\Delta\vec{F}_{a_{\delta_e}}^{(k)}$, the net aerodynamic pitching moment $\vec{M}_a^{(k)}$, gravitational force $\vec{F}_g^{(k)}$ (at strip CG), inertial force $\vec{F}_i^{(k)}$ (at strip CG), and moment $\vec{M}_i^{(k)}$, as well as the reaction forces $\vec{F}_r^{(k)}$, $\vec{F}_r^{(k+1)}$ and moments $\vec{M}_r^{(k)}$, $\vec{M}_r^{(k+1)}$ at the two ends.

The origins O_k and O_{k+1} of the two local coordinate systems are located on a defined elastic axis, and the three directions are aligned with the three global axes of the aircraft. The origins of the axes at the k and $k+1$ boundaries are shifted due to taper ratio, dihedral (or anhedral), sweep and thickness-to-chord variation. To find the reaction forces $\vec{F}_r^{(k+1)}$, a simple force balance is used:

$$\vec{F}_r^{(k+1)} - \vec{F}_r^{(k)} + \vec{F}_{a,0}^{(k)} + \Delta\vec{F}_{a_{\delta_e}}^{(k)} + \vec{F}_i^{(k)} + \vec{F}_g^{(k)} = \vec{0}. \tag{36}$$

To compute the reaction moment $\vec{M}_r^{(k+1)}$, the moment balance involves additional terms due to the placement of the forces. As seen in Figure 11, $\vec{\tilde{r}}_r^{(k)}$ is the vector from origin O_{k+1} to origin O_k, $\vec{\tilde{r}}_{a,0}^{(k)}$ is the vector from O_{k+1} to the strip aerodynamic center, $\vec{\tilde{r}}_{a_{\delta e}}^{(k)}$ is the vector from O_{k+1} to the location where the incremental aerodynamic force $\Delta\vec{F}_{a_{\delta_e}}^{(k)}$ acts, and $\vec{\tilde{r}}_{cg}^{(k)}$ is the vector from O_{k+1} to the strip center of gravity. The tildes are used to distinguish between position vectors for each strip versus position vectors for the aircraft. The moment balance equation is then given by

$$\vec{M}_r^{(k+1)} - [\vec{M}_r^{(k)} + \vec{\tilde{r}}_r^{(k)} \times \vec{F}_r^{(k)}] + [\vec{M}_{a,0}^{(k)} + \vec{\tilde{r}}_{a,0}^{(k)} \times \vec{F}_{a,0}^{(k)}] + [\vec{\tilde{r}}_{a_{\delta e}}^{(k)} \times \Delta\vec{F}_{a_{\delta e}}^{(k)}] + [\vec{M}_i^{(k)} + \vec{\tilde{r}}_{cg}^{(k)} \times \vec{F}_i^{(k)}] + [\vec{\tilde{r}}_{cg}^{(k)} \times \vec{F}_g^{(k)}] = \vec{0}. \tag{37}$$

The position vectors $\vec{\tilde{r}}_r^{(k)}$ and $\vec{\tilde{r}}_{cg}^{(k)}$ for each strip are time independent, but $\vec{\tilde{r}}_{a_{\delta e}}^{(k)}$ and $\vec{\tilde{r}}_{a,0}^{(k)}$ are computed at each time step based on the location of the aerodynamic centers. For the case of symmetric airfoils, $\vec{M}_{a,0}^{(k)} = 0$.

To understand the major contributors to the root forces and moments, equilibrium is also applied for the entire horizontal tail at once, using the same equilibrium equations as those used for each strip. The only difference is that the position vectors of the point of application of all the forces are calculated relative to the horizontal tail root. By applying this procedure at each time step, the time histories of the reaction load between the structure and the horizontal tail are decomposed into aerodynamic and inertial components.

III.B. Inertial Loads

The concept of inertial loads allows for the generalization of equilibrium, which is fundamentally a statics concept, to the case of dynamics problems through D'Alembert's principle and the notion of *dynamic equilibrium*. In fact, Eq. 36 and Eq. 37 enforce the condition of dynamic equilibrium of the strip. The equations of motion of strip 'k', subjected to *externally applied* forces $\sum \vec{F}_{ext}^{(k)}$ and moments $\sum \vec{M}_{ext}^{(k)}$, are given by

$$\begin{aligned}
\sum \vec{F}_{ext}^{(k)} &= m_{strip}^{(k)}\, \vec{a}_{strip}^{(k)} \implies \sum \vec{F}_{ext}^{(k)} + \left[- m_{strip}^{(k)} \vec{a}_{strip}^{(k)} \right] = \vec{0} \\
\sum \vec{M}_{ext}^{(k)} &= \bar{\bar{I}}_{strip}^{(k)}\, \dot{\vec{\omega}} + \vec{\omega} \times \left(\bar{\bar{I}}_{strip}^{(k)}\, \vec{\omega} \right) \implies \sum \vec{M}_{ext}^{(k)} + \left[- \bar{\bar{I}}_{strip}^{(k)}\, \dot{\vec{\omega}} - \vec{\omega} \times \left(\bar{\bar{I}}_{strip}^{(k)}\, \vec{\omega} \right) \right] = \vec{0}.
\end{aligned} \tag{38}$$

By definition, the inertial loads, namely the inertial force $\vec{F}_i^{(k)}$ and the inertial moment $\vec{M}_i^{(k)}$, enforce the dynamic equilibrium conditions $\sum \vec{F}_{ext}^{(k)} + \vec{F}_i^{(k)} = \vec{0}$ and $\sum \vec{M}_{ext}^{(k)} + \vec{M}_i^{(k)} = \vec{0}$. They are equal to the terms within brackets in Eq. 38. Thus, the inertial force $\vec{F}_i^{(k)}$ and moment $\vec{M}_i^{(k)}$ acting on strip 'k' are given by

$$\begin{aligned}
\vec{F}_i^{(k)} &= -m_{strip}^{(k)} \vec{a}_{strip}^{(k)} \\
&= -m_{strip}^{(k)} \left[\dot{\vec{V}}_0 + \vec{\omega} \times \vec{V}_0 + \cancelto{0}{\ddot{\vec{r}}_{strip}^{(k)}} + \dot{\vec{\omega}} \times \vec{r}_{strip}^{(k)} + 2\vec{\omega} \times \cancelto{0}{\dot{\vec{r}}_{strip}^{(k)}} + \vec{\omega} \times (\vec{\omega} \times \vec{r}_{strip}^{(k)}) \right], \qquad (39) \\
\vec{M}_i^{(k)} &= -\bar{\bar{I}}_{strip}^{(k)}\, \dot{\vec{\omega}} - \vec{\omega} \times \left(\bar{\bar{I}}_{strip}^{(k)}\, \vec{\omega} \right), \qquad (40)
\end{aligned}$$

where $\vec{V}_0 = \{u, v, w\}^T$ is the velocity of the aircraft reference point O, $\vec{\omega} = \{p, q, r\}^T$ is the aircraft angular velocity, and $\vec{r}_{strip}^{(k)}$ is the strip's CG position relative to the aircraft reference point O. The time derivatives of

the position vector $\vec{r}_{strip}^{(k)}$ are zero since the strip's CG location is assumed to be fixed relative to the reference point. It is worth noting that this inertial force depends on the mass properties of the strip (through $m_{strip}^{(k)}$), the position of the mass element (through $\vec{r}_{strip}^{(k)}$), and on the kinematics of the aircraft (through $\vec{V}_0$, $\dot{\vec{V}}_0$, $\vec{\omega}$, and $\dot{\vec{\omega}}$). These calculations are performed for every simulation time step, resulting in time histories of the inertial forces and moments on each strip of the horizontal tail.

III.C. Aerodynamic Loads

Each horizontal tail section experiences a normal force and a pitching moment due to the angle of attack of the tail as well as an incremental force contribution due to the elevator deflection, as shown in Figure 11. These are calculated using normalized coefficients as

$$N_{strip}^{(k)} = \overline{q} * C_{N,strip}^{(k)} * S_{strip}^{(k)} \tag{41}$$

$$M_{strip}^{(k)} = \overline{q} * C_{m,strip}^{(k)} * S_{strip}^{(k)} * \bar{c}_{strip}^{(k)} \tag{42}$$

$$\Delta N_{strip}^{(k)} = \overline{q} * \Delta C_{N,strip,\delta_e}^{(k)} * S_{strip}^{(k)} \tag{43}$$

Each coefficient is computed as a buildup that accounts for the angle of attack seen by the tail.

$$C_{N,strip}^{(k)} = C_{N_0}^{(k)} + C_{N_i}^{(k)} \alpha_t \tag{44}$$

$$C_{m,strip}^{(k)} = C_{m_0}^{(k)} + C_{m_i}^{(k)} \alpha_t \tag{45}$$

$$\Delta C_{N,strip,\delta_e}^{(k)} = C_{N_{\delta_e}}^{(k)} \delta_e \tag{46}$$

where α_t is calculated as described in equation 7. The aerodynamic center is dependent on the Mach number for both the normal force and the contribution due to elevator deflection. Thus, the location of these forces (in terms of percentage of the chord) is computed by interpolating based on the Mach number at each time step. The WL and BL coordinates for each strip's aerodynamic center are independent of time and are known from the horizontal tail geometry.

IV. Results and Discussion

Results are presented to show (i) control input, control effort, and load factor during the execution of the maneuver (Section IV.A) and (ii) structural shear and bending loads developed during the maneuver (Section IV.B). For continuity of presentation, the observations are discussed using a subset of the test cases that were evaluated. Results for additional test cases are presented in appendices for the interested reader.

IV.A. Maneuver Simulation

After both nose up and nose down checked pitch maneuvers were simulated for all 231 test points, the required control histories were analyzed. For the nose up maneuver, only one case required that the pilot hold the yoke control input at maximum. This case, shown in Figure 13, corresponds to the heavyweight configuration with maneuver initiation at ceiling altitude and dive speed. All other nose up cases required an amplitude scale-down of the control input in order to avoid exceeding the positive limit load factor. For the nose down checked pitch maneuver, three cases required maximum control input to be held: the same case as described above and two directly adjacent cases in the Mach-altitude testing envelope.

Due to the design of the pilot model (output-saturated PID control scheme), the control column force stayed within the ranges specified in FAR §25.397 for all simulated cases. Figure 18 shows heatmaps of the maximum pilot control force $\max(|F|)$ required across the testing envelope for the three weight conditions. As expected, heavier configurations require control forces of larger magnitude. The control force magnitudes are largely driven by the dynamic pressure, with the most significant efforts required by the pilot at high Mach numbers. For a fixed Mach number, the maximum pilot effort decreases with altitude as the density (thus, dynamic pressure) decreases.

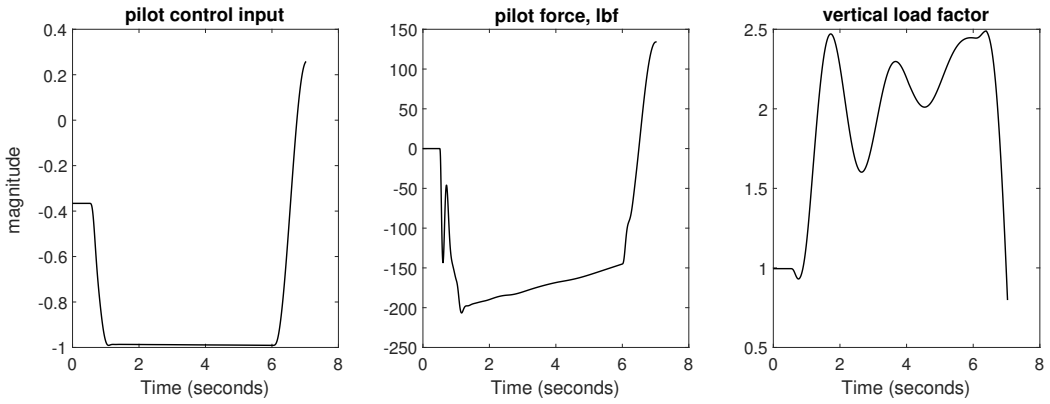

Figure 13: Pilot control input (left), control column force (middle) and vertical load factor (right) for heavyweight configuration at ceiling altitude and maneuvering dive speed. The deflection of the yoke is maximum (-1) and held for 5 seconds. Following the elevator input, short period and phugoid oscillations are excited during the hold period, during which the force required by the pilot slowly decreases with time.

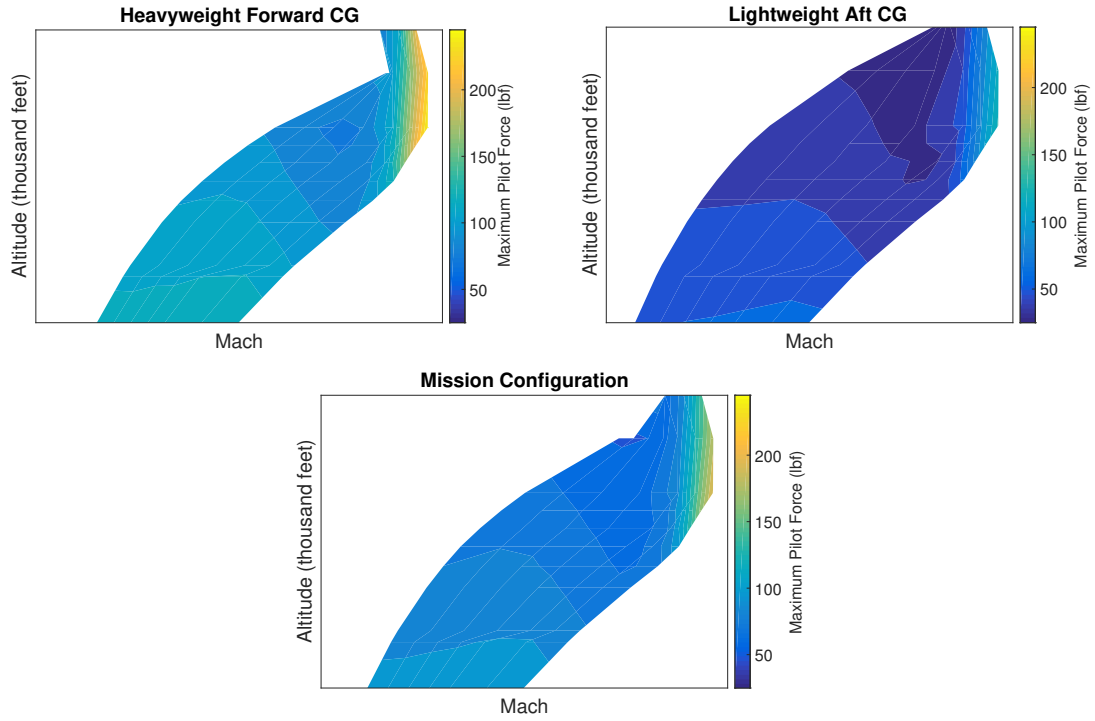

Figure 14: Maximum pilot force during the nose up checked pitch maneuver over all cases

IV.B. Structural Loads Analyses

For each altitude-Mach-weight combination that was simulated, the structural loads processing approach yielded the time histories of both the sectional and root loads as well as the elevator hinge moment during both nose up and nose down checked pitch maneuvers. Figure 15 shows the evolution of the elevator hinge moment, root bending moment, and root vertical shear force during a nose up checked pitch maneuver. The individual contributions of aerodynamic, inertial, and gravitational loads to the root loads are displayed as well. The plots correspond to the loads experienced at the root of the starboard horizontal stabilizer (and exerted by it on the aircraft structure).

When the nose-up maneuver starts, the trailing-edge up elevator deflection generates a net downward load on the horizontal stabilizer, which makes the airplane pitch up. Since the tail initially accelerates downward,

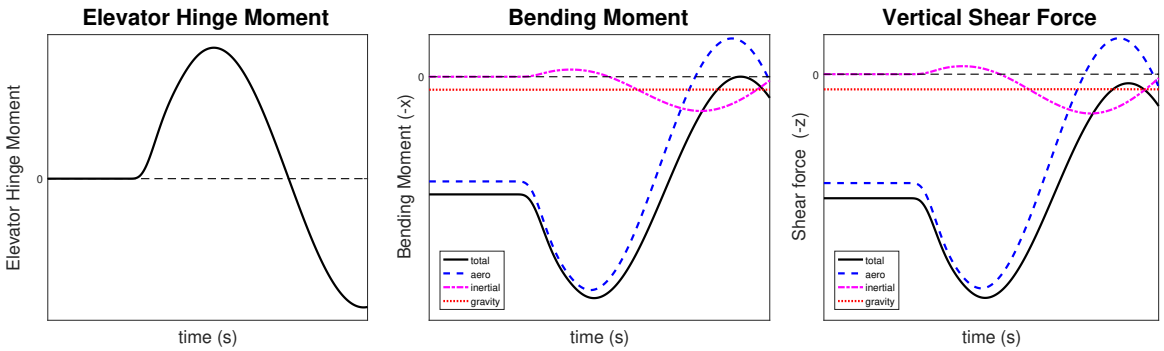

Figure 15: Variation of elevator hinge moment, root bending moment, and root vertical shear force during a nose up checked pitch maneuver

the inertial forces and moments tend to resist that, and thus they increase in the first part of the maneuver. The weight of the tail is constant in magnitude and the change in the component of the weight along the WL-axis is several orders of magnitude smaller than the aerodynamic force. Thus, this type of load appears as fairly constant in the WL direction, when plotted against all other forces. The contributions to the root bending moment follow the same trends as the shear forces and are primarily driven by the aerodynamic load.

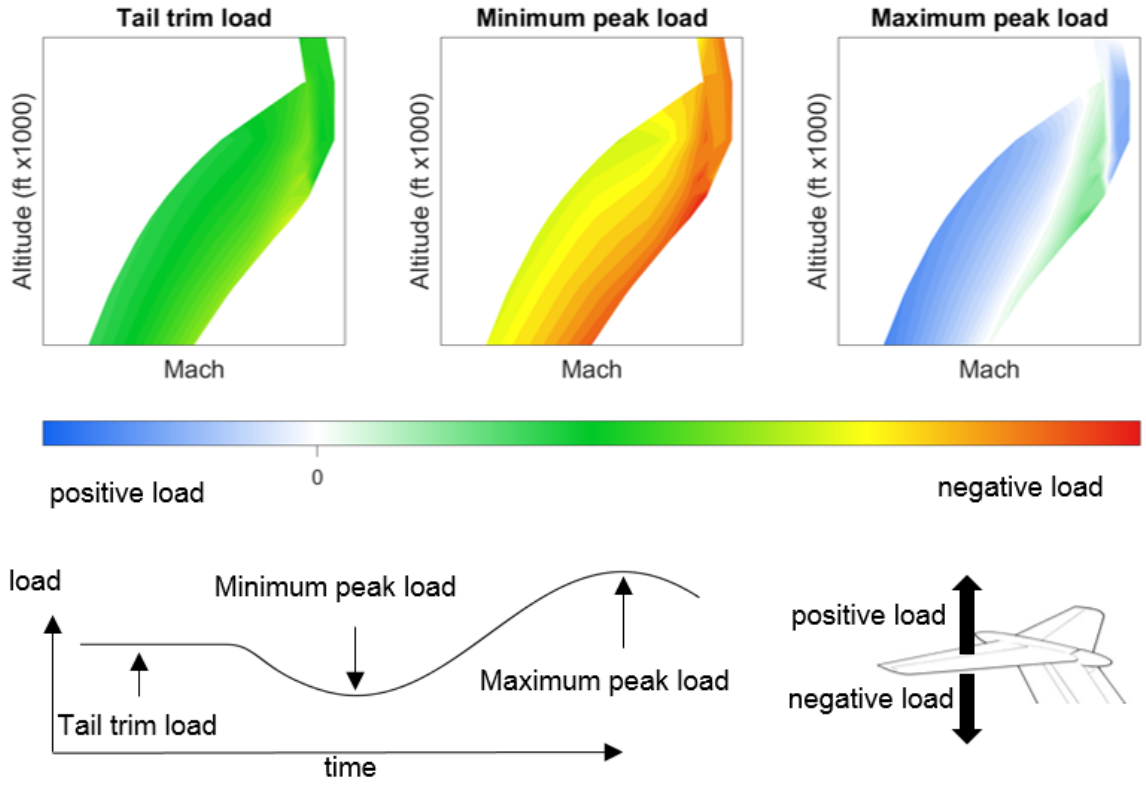

Figure 16: Vertical root shear load across the testing envelope for the heavyweight forward CG during the nose up checked pitch maneuver

After the minimum and maximum peak loads are identified from the time histories of each test case, heatmaps of extrema peak loads can be overlaid on the testing envelope. Figure 16 shows the peak vertical shear loads across the testing envelope at three epochs during the nose up checked pitch maneuver in the heavyweight forward CG configuration. This weight configuration was seen to develop the most severe loads

for the aircraft (therefore, results for the mission configuration and the lightweight aft CG are deferred to the appendices). The left plot shows the load during trimmed flight (prior to initiation of the maneuver). At trim, the horizontal stabilizer is lightly loaded with a downward (negative) load. The center plot shows the minimum peak load, in other words, the magnitude of the most negative load in the entire time history. This occurs during the pitch-up phase of the maneuver. Finally, the right plot shows the maximum peak load, in other words, the magnitude of the most positive load in the entire time history. This occurs while the maneuver is being checked. The white zones on the maximum peak load plot show cases where the stabilizer is off-loaded during the checking of the maneuver. Figure 17 shows results in the same format for the extreme stabilizer root bending moments during the nose-up maneuver for the same weight configuration. As expected, there is a correlation between the bending moment and the vertical shear force trends. Additionally, results for the vertical shear force and bending moments during the nose down maneuvers are also given in the appendices. The analysis also yields time histories and extrema for the torsion loads at the stabilizer root, but these are not presented for sake of brevity.

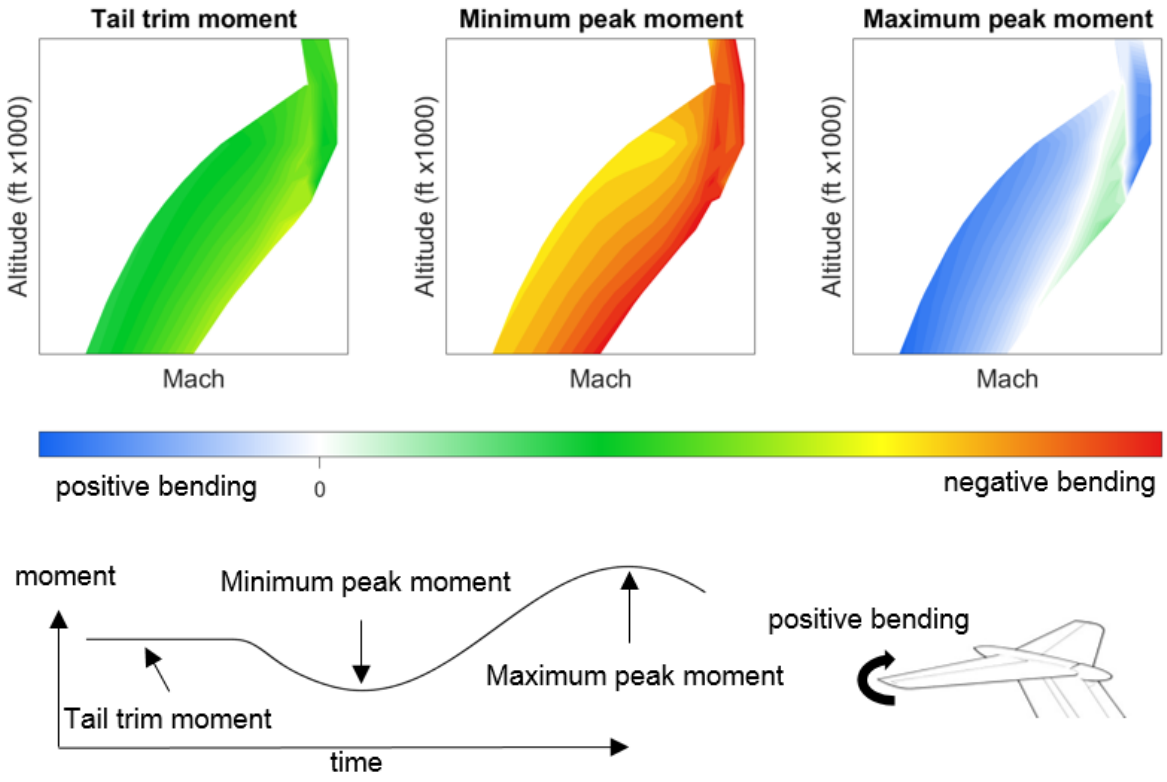

Figure 17: Root bending moment across the flight envelope for the heavyweight forward CG during the nose up checked pitch maneuver

Collective analysis of the load time histories for all altitude-Mach and weight configurations and for both nose up and nose down checked pitch maneuvers allows the identification of the most constraining structural load cases imposed by FAR §25.331(c)(2) requirements. The most critical shear force and bending moment at the stabilizer root were achieved for the heavyweight condition and during the nose-up maneuver. The largest downward force occurs when the nose up maneuver is initiated at design dive speed for a middle range altitude. This flight condition already has a relatively large downward trim load which is further incremented by the high dynamic pressure. The largest upward force on the stabilizer happens at sea-level and at maneuvering speed. This flight condition is almost off loaded at trim and therefore can result in a positive load after the maneuver is checked. The critical points are identical in terms of both shear force and bending moment.

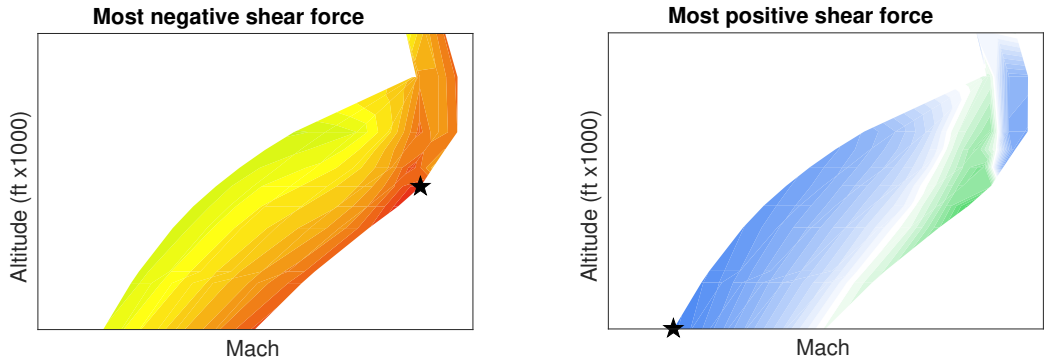

Figure 18: Most negative (left) and most positive (right) shear force on the horizontal stabilizer is identified by a black pentagram. The color scale is the same has for Fig.16

V. Conclusions and Future Work

In this work, a framework was developed to facilitate the evaluation of structural loads developed during dynamic maneuver requirements specified within the Federal Aviation Regulations (FARs). The framework comprises two main parts: (1) a flight dynamics simulation model that includes a model of the human pilot, a simplified model of the flight control system, and has the ability to incorporate maneuver control logic based on FARs and (ii) a loads analysis module to calculate time histories of structural loads developed during the maneuvers and identify critical load cases. The framework was tested for the case of a business jet performing a checked pitch maneuver, specified in FAR §25.331(c)(2). The work was done with technical oversight provided by subject-matter experts from Gulfstream Aerospace Corporation, and with aircraft-specific data for an existing aircraft from the organization's product line.

The testing envelope for the maneuver was first discretized into altitude-Mach combinations. For each such test point and for three representative weight/loading configurations, the framework was used to simulate both nose up and nose down checked pitch maneuvers. The time histories of the airplane's kinematic variables were then used by the loads analysis module to compute corresponding time histories of structural shear, bending, and torsion loads developed on the horizontal stabilizer. Inspection of these load histories allowed the identification of the flight and weight/loading conditions that resulted in the most constraining empennage loads.

Avenues for future work utilizing and extending the capabilities of the developed framework include (i) loads development for other structural parts (e.g., wing, vertical stabilizer, etc.), (ii) simulation of other maneuvers (e.g., lateral/directional maneuvers in addition to other longitudinal ones), (iii) accounting for structural flexibility through flex-to-rigid ratios or additional elastic states, and (iv) assessment of the impact of uncertainty in aerodynamic characteristics or mass properties on predicted maneuver loads.

Acknowledgements

The authors would like to thank and acknowledge the following representatives from the Gulfstream Aerospace Corporation in Savannah, Georgia for their technical guidance and oversight during the course of this work: Mr. Robert Martin (Engineering Manager - Loads, Dynamics, & Mass Properties), Mr. Mark Ray (Staff Scientist - Loads & Dynamics), Mr. James Senter (Group Head - Loads & Dynamics), and Mr. Philip Riek (Engineer - Loads & Dynamics).

References

[1]Mares, C. and Ursache, N., "Aircraft Ground Structural Testing," *Encyclopedia of Aerospace Engineering*, Vol. 1-16, 2014.

[2]De Florio, F., *Airworthiness: an introduction to aircraft certification*, Elsevier, 2010.

[3]Mohaghegh, M., "Validation and certification of aircraft structures," *46th AIAA/ASME/ASCE/AHS/ASC Structures, Structural Dynamics and Materials Conference*, 2005, p. 2162.

[4]Xie Jian, L. Y., "Study on Airworthiness Requirements of Composite Aircraft Structure for Transport Category Aircraft in FAA," *Procedia Engineering*, Vol. 17, 2011, pp. 270–278.

[5]Wright J. R., C. J. E., *Introduction to Aircraft Aeroelasticity and Loads*, John Wiley & Sons Australia, Limited, 2015.

[6]Federal Aviation Administration, U. D. o. T., "Code of Federal Regulations, Title 13, Part 25: Airworthiness Standards: Transport Category Airplanes," `http://www.ecfr.gov`, [Online; accessed 26-October-2016].

[7]Chakraborty, I., Lozano, B., and Mavris, D. N., "Pilot-Friendliness Considerations for Personal Air Vehicle Flight Control Systems," *15th AIAA Aviation Technology, Integration, and Operations Conference*, 2015, pp. 6–17.

[8]Etkin, B., *Dynamics of flight: stability and control*, John Wiley & Sons Australia, Limited, 1982.

[9]Lambe, A. B. and Martins, J. R., "Extensions to the design structure matrix for the description of multidisciplinary design, analysis, and optimization processes," *Structural and Multidisciplinary Optimization*, Vol. 46, No. 2, 2012, pp. 273–284.

[10]Kolk, W. R., *Modern flight dynamics*, Prentice Hall, 1961.

[11]Cook, M. V., *Flight dynamics principles: a linear systems approach to aircraft stability and control*, Butterworth-Heinemann, 2012.

Appendix A: Nose up maneuver results

Vertical shear force

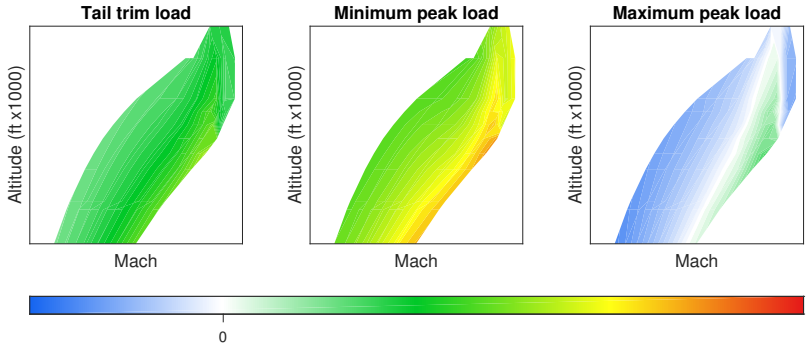

Figure 19: Vertical root shear force for the nose up checked-pitch maneuver - Mission weight configuration

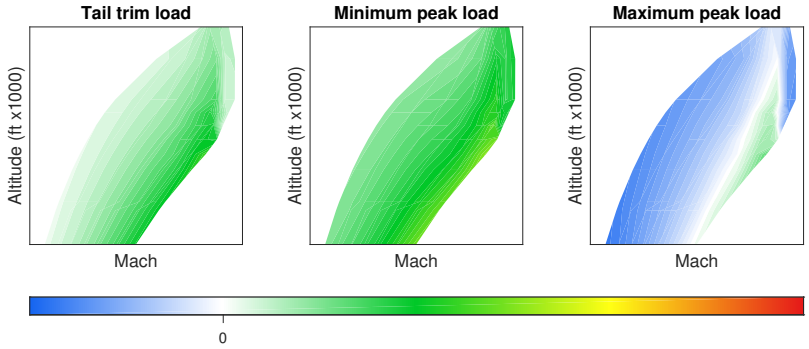

Figure 20: Vertical root shear force for the nose up checked-pitch maneuver - Lightweight aft CG configuration

Bending moment

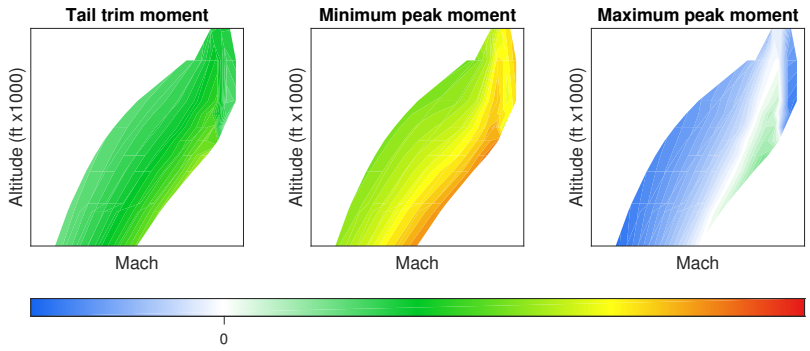

Figure 21: Root bending moment for the nose up checked-pitch maneuver - Mission weight configuration

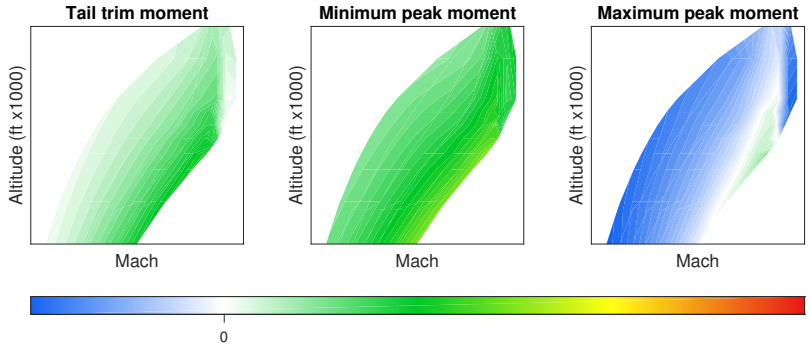

Figure 22: Root bending moment for the nose up checked-pitch maneuver - Lightweight aft CG configuration

Appendix B: Nose down maneuver results

Vertical shear force

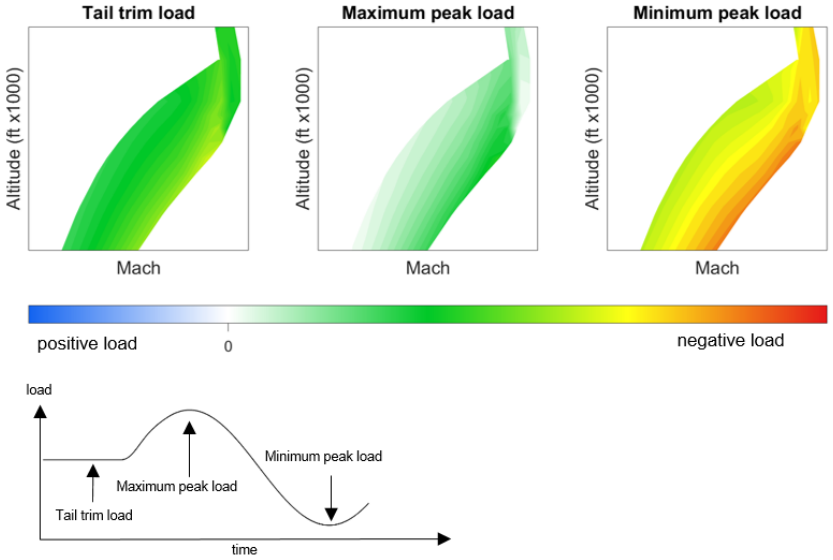

Figure 23: Vertical root shear force for the nose down checked-pitch maneuver - Heavyweight configuration

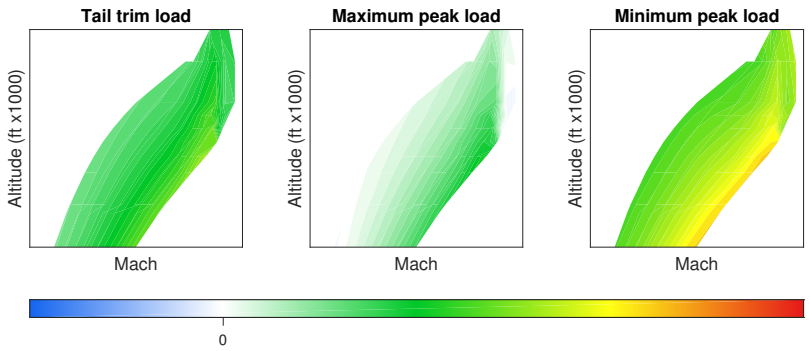

Figure 24: Vertical root shear force for the nose down checked-pitch maneuver - Mission weight configuration

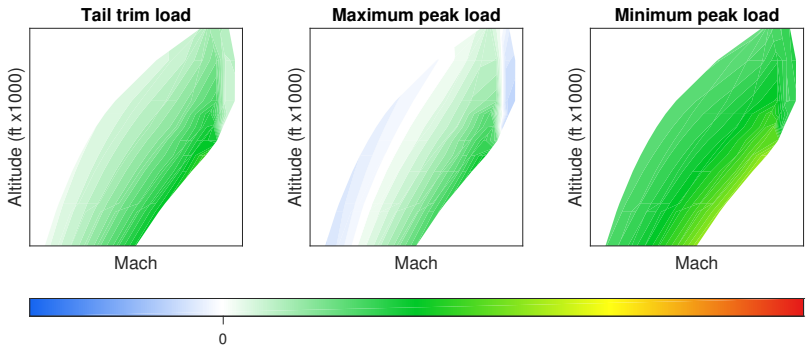

Figure 25: Vertical root shear force for the nose down checked-pitch maneuver - Lightweight aft CG configuration

Bending moment

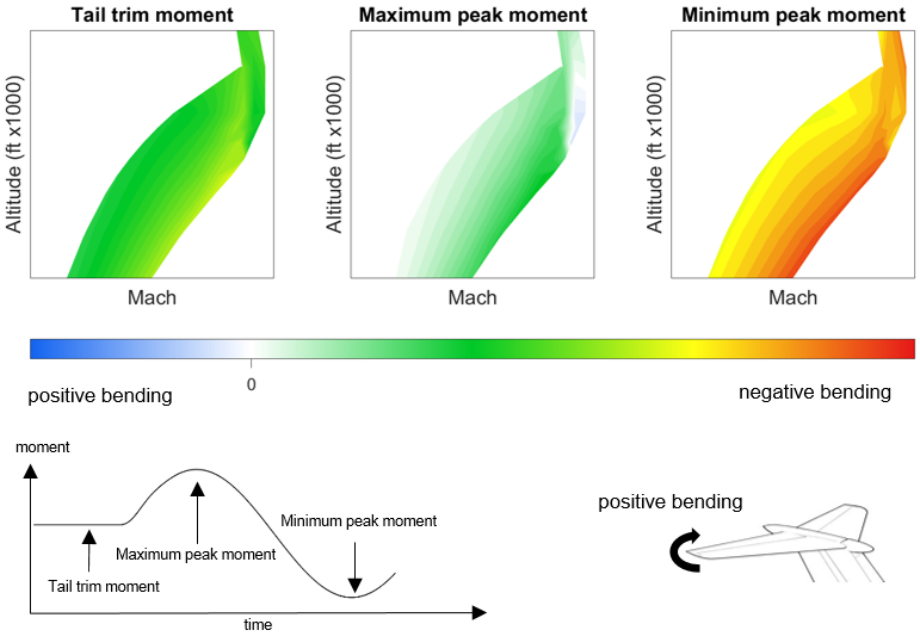

Figure 26: Root bending moment for the nose down checked-pitch maneuver -Heavyweight forward CG configuration

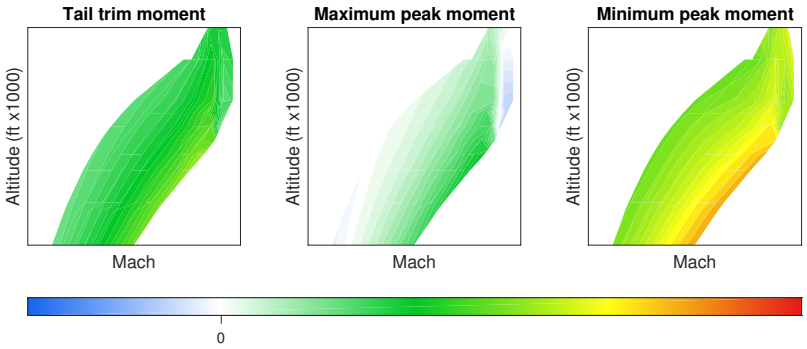

Figure 27: Root bending moment for the nose down checked-pitch maneuver - Mission weight configuration

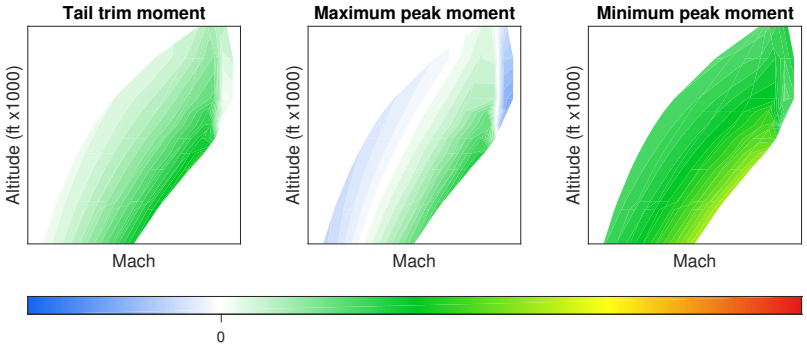

Figure 28: Root bending moment for the nose down checked-pitch maneuver - Lightweight aft CG configuration